

Similarities between Wheels and Tracks: A “Tire Model” for Tracked Vehicles

RuiZeng Zhang, Wei Zhou, *Senior Member, IEEE*, Haiou Liu, Jianwei Gong, *Member, IEEE*,
Huiyan Chen and Amir Khajepour, *Member, IEEE*

Abstract—As an important component of land transportation systems, tracked vehicles (TRVs) and wheeled vehicles (WVs) have developed independently in parallel, particularly in the modeling of vehicle-ground interactions. However, their differences are not as significant as they appear. This paper introduces a simplified terramechanics-based track-ground interaction model for the motion control of TRVs on firm ground. The simplified interaction model addresses the problem that the terramechanics-based models are too complex to be applied to optimization-based real-time control algorithms. Interestingly, the proposed track-ground interaction model closely resembles to the tire model used for WVs. Through comparison, we present the unified mechanisms underlying vehicle-ground interactions. In our approach, TRVs can be treated as a special type of skid-steer WVs, which benefits the theories and methods of wheel vehicles to be deployed in the TRV domain. Finally, we verify the proposed interaction model with extensive dynamic data from a real dual motor-driven TRV to demonstrate its effectiveness.

Index Terms—Tracked vehicle, Dynamic model, Terramechanics theory.

I. INTRODUCTION

A N effective and efficient dynamic model is fundamental to modern control theory; however, in the field of tracked vehicles (TRVs) there is no such a ready-made model for dynamic motion control, just like the tire model for wheeled vehicles (WVs) [1], [2]. The model’s “absence” hinders the development of precise dynamic control for TRVs. Consequently, the question arises: is there a “tire model” for TRVs?

Tracks not only endow TRVs with excellent road adaptability [3], enabling them to perform heavy-duty tasks in mining [4], agriculture [5], construction [6], disaster relief [7], etc., but also introduce complex vehicle-ground interaction. Imagine calculating the forces and resistance moment in a rectangular stress area where the normal pressure is unevenly distributed and the shear stress depends on past displacement and changes in normal pressure. The common approach is to use numerical

Copyright (c) 2024 IEEE. Personal use of this material is permitted. However, permission to use this material for any other purposes must be obtained from the IEEE by sending a request to pubs-permissions@ieee.org.

This work was supported in part by Key Laboratory of Intelligent Unmanned Systems Technology and the National Natural Science Foundation of China under Grant 52172378. (Corresponding author: Jianwei Gong.)

R. Zhang, H. Liu, J. Gong and H. Chen are with the School of Mechanical Engineering, Beijing Institute of Technology, Beijing 100081, China (email: hireason@163.com, gongjianwei@bit.edu.cn)

W. Zhou is with the School of Computer Science and Informatics, Cardiff University, Cardiff CF24 4AG, United Kingdom (email: zhouw26@cardiff.ac.uk).

A. Khajepour is with the Department of Mechanical and Mechatronics Engineering, University of Waterloo, Waterloo, ON N2L 3G1, Canada (email: a.khajepour@uwaterloo.ca).

integration, as employed by terramechanics-based dynamic analysis models [8]–[11]. In these models, shear stress at each point of the track is calculated based on the shear stress-shear displacement relationship, and overall forces are derived by the numerical integration. However, the numerical integration process may lose gradient information and lead to a complex model, causing difficulty in real-time dynamic motion control. Alternatively, commonly used control models for TRVs include kinematic model [12], [13] or dynamic model based on friction theory [14]–[16]. Nevertheless, kinematic models are challenging to apply safety dynamic constraints, and friction theory is limited in modeling the soil shearing of large TRVs [8]. Therefore, achieving desirable autonomous driving for TRVs necessitates overcoming the significant challenge of handling the complex track-ground interaction [17].

Let us revisit the function of tracks to answer the question, “Is there a ‘tire model’ for TRVs?”. Tracks disperse wheel-ground pressure on soft ground, enabling TRVs to handle muddy roads effectively. However, most roads are dry and firm. On firm ground, the pressure disperse effects of the tracks are negligible because both the ground deformation and the track tension are limited. Theoretically, greater track tension results in a more even the track-ground pressure. However, track tension is typically kept within a reasonable range to ensure durability and prevent derailing. Experimental results and related literature [18] demonstrate that on firm ground, the track-ground pressure is concentrated on a limited area beneath the road wheels, which is similar to WVs. Therefore, it is feasible to propose a “tire model” for TRVs on firm ground using the methodology of WVs.

In this paper, we shift our focus from the shear stress on each point of the track to the overall forces through equivalent substitution. By theoretical derivation, we propose a “tire model” for TRVs based on terramechanics theory. Subsequently, we formulate a slip-aware dynamic model for TRVs on firm ground using this “tire model”. This approach avoids numerical integration and is suitable for model-based dynamic motion control. We use the term “tire model” to refer to the track-ground interaction model due to the similarity between the track-ground interaction model and the actual tire model in WVs.

The main contributions of this work are summarized as follows:

- (1) Proposing a simplified “tire model” for TRVs on **firm ground**, enabling the application of terramechanics-based theory in motion control of TRVs. Based on this “tire

model” and the characteristics of TRVs, a dual-track model considering track slip is formulated.

- (2) Comparing the proposed TRV “tire model” with the tire model of WVs to reveal the underlying relationship between tracks and wheels.
- (3) Verifying the proposed terramechanics-based dynamic model with various soil and experimental maneuvers of a bilateral motor-driven TRV.

The rest of the paper is organized as follows. In Section II, we discuss related work on TRV modeling and demonstrate the research gaps. The “tire model” and a dynamic model for TRVs are presented in Section III. Then, a comparison between the proposed “tire model” and the UniTire model is made in section IV. The experimental results and analysis are given in section V, and the conclusion and prospects are drawn in the last section.

II. RELATED WORK

In this section, related work about the modeling of TRVs and WVs will be discussed respectively. The related models for TRVs will be discussed in detail to demonstrate the research gaps and the need of a “tire model” for TRVs. Additionally, a brief overview of tire models for WVs will be provided for comparison.

A. Related Models for TRVs

Currently, models for TRVs can be classified into three categories: kinematic models, friction-based dynamic models and terramechanics-based dynamic models. Each of these models has its own advantages and disadvantages that can not be overlooked.

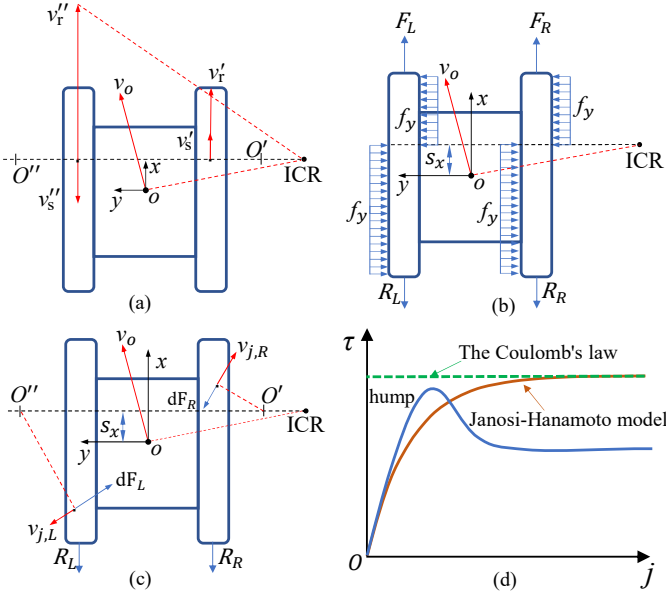


Fig. 1. Different types of models for TRVs: (a) the kinematic model, (b) the friction-based dynamic model, (c) the terramechanics-based dynamic model and (d) the shear stress-shear displacement relationship.

The kinematic model is one of the most commonly used models for TRVs, widely applied in path planning [19], trajectory tracking [12], [20]–[22], and slip parameter estimation

[17], [23]–[25]. As shown in Fig. 1 (a), the coordinate system x - y is fixed at the center of gravity (CoG), and the point ICR is the instantaneous center of rotation. Points O' and O'' are instantaneous centers of the tracks slipping on the ground on both sides [8]. The track slip is inevitable during turning. Experimental results [26] indicate that ignoring track slip leads to theoretical turning radius and resistance will be about 40% smaller and 50% larger than actual values, respectively. The smaller the turning radius, the more pronounced the slip. Therefore, the kinematic model is usually paired with the slip estimation algorithm. Slip parameter estimation algorithms, including the least squares method [27], extended Kalman filter [12], [17], [23], [24], Levenberg-Marquardt algorithm [19] and etc., are typically used to estimate the slip velocity v_s on both tracks and longitudinal ICR offset s_x . Although good estimation results can be achieved, these estimation algorithms cannot predict future slip, which is essential for model-based controllers like model predictive control (MPC). Despite its concise form and ease of implementation, the kinematic model may fail when dynamics-related information dominates control performance, such as high speed or low adhesion scenario [28]. Additionally, in kinematic models, vehicle lateral slip v_y is an uncontrolled variable of the control inputs. The sprocket speeds have no direct contribution on lateral slip.

The friction-based dynamic model is the mainstream in dynamic control for TRVs, as shown in Fig. 1 (b). The relationship between shear displacement j and shear stress τ according to Coulomb’s law of friction is shown in Fig. 1 (d), where the maximum track-ground shear stress occurs simultaneously with the relative displacement [8]. Although extensive experimental evidence demonstrates that the track-ground shear stress is related to shear displacement [29], [30], friction theory-based dynamic models are generally applicable [8]. The dynamic model is linear, assuming a constant lateral friction coefficient, which overcomes the limitations of the kinematic model that cannot impose dynamic constraints. However, the constant lateral friction coefficient may oversimplify the actual track-ground interaction of large TRVs on firm ground [8]. The Nikitin empirical formula [14] assumes the lateral friction coefficient is a function of turning radius, making it more suitable for large TRVs. However, some parameters in this formula lack a clear physical meaning and can only be determined experimentally. In addition, the Nikitin empirical formula assumes the turning resistance moment is independent of vehicle velocity, but our experimental results demonstrate that velocity affects the turning resistance moment, especially when the turning radius is small.

The terramechanics-based dynamic model, illustrated in Figs. 1 (c) and (d), is primarily used for dynamic analysis. In the field of WVs, tire forces are estimated by the tire model directly treating the tire as a whole; nevertheless, researchers in the field of TRVs estimate the track-ground force by integrating or summing shear stress. The terramechanics-based dynamic model is supported by extensive experimental data and has been proven to accurately represent actual track-ground interactions. However, its complex form, particularly the numerical integration, limits its application in fields requir-

TABLE I
CLASSIFICATION OF MODELS FOR TRVs AND THEIR APPLICATIONS

| Type | Features | Usage | Application | Verification |
|--|---|---|---|--|
| Kinematic model | Ignore longitudinal slip | Path tracking [4], [31]–[33] | Small TRVs [31] Agriculture TRVs [32] Sea mining TRVs [4] Unspecified [33] | Real car [31] Simulation [4], [32], [33] |
| | Consider track longitudinal slip | Path planning [19] Parameter estimation [17], [23]–[25] Path tracking [3], [12], [20]–[22], [34]–[36], [27] | Large TRVs ¹ [12], [19], [20], [25], [36] Small TRVs ² [3], [17], [22], [23], [35] Sea mining TRVs [21] Unspecified [27], [34] | Real car [3], [12], [17], [19], [23], [24], [27], [36] Simulation [20]–[22], [25], [34], [35] |
| The friction-based dynamic model | Assume the friction coefficient is a constant, e.g. the Coulomb's law of friction | Dynamics control [16], [15], [37]–[43] Dynamics analysis [44] Parameter estimation [45], [46] | Large TRVs [38], [40], [41], [43], [45] Small TRVs [37], [15], [16], [39], [42], [44], [46] | Real car [37], [15], [44], [46] Simulation [16], [38]–[43], [45] |
| | Assume the lateral friction coefficient is related to turning radius, e.g. Nikitin formula | Dynamics control [47], [48] Energy management [49]–[51] | Large TRVs [47], [49], [50] Small TRVs [48] Unspecified [51] | Real car [48] Simulation [47], [49]–[51] |
| The terramechanics-based dynamic model | Assume track-ground pressure is evenly or partly evenly distributed | Dynamics analysis [8], [9], [26], [52]–[54] | Large TRVs [8], [9], [26], [52], [54] Small TRVs [53] | Real car [8], [9], [26], [52]–[54] |
| | Assume the shear displacement is the same in a limited area, and changed the integral to discrete summation | Dynamics analysis [55], [56] | Large TRVs [55] Sea mining TRVs [56] | Real car [55] Simulation [56] |

¹ Means TRVs that track gauge is bigger than 1.5m;² Means TRVs that track gauge is smaller than 1.5m;

ing high real-time performance, such as path tracking. Due to this complexity, the model is generally simplified during the modeling process. For example, assuming the track-ground pressure is evenly [8] or partly evenly distributed [55]. Despite these simplifications, numerical integration or discrete summation cannot be avoided, making the terramechanics-based dynamic model challenging to use in model-based controllers like linear quadratic regulator (LQR) and MPC. The shear displacement-shear stress relationship model is the core of the terramechanics-based dynamic model. Among the various models, the Janosi-Hanamoto model [57] shown in Fig. 1 (d) is the most wildly used due to its concise form and ease of implementation. It performs well on loose sand, saturated clay, dry fresh snow, and most distributed soils, but cannot describe the "hump" phenomenon that occurs on dense sand, silt and frozen snow [58]. Alternative models proposed by J.Y. Wong [59], M.G. Bekker [60] and others can describe the "hump" but are much more complex than the Janosi-Hanamoto model. In addition, the shear displacement is the accumulation of

the past shear velocity. Thus, the vehicle states are generally assumed to be constant to simplify the process, which limits the model's usage in non-steady states. Consequently, the numerical integration form and the complex terramechanics model restrict the use of the terramechanics-based dynamic model in real-time dynamic control applications.

In summary, existing models for TRVs each have their advantages, but balancing accuracy and complexity to achieve precise real-time motion control of large TRVs remains challenging. Similar conclusions can be drawn from the statistical data in Table I. The kinematic model is predominantly applied in path tracking, as reported in the literature surveyed. Models that ignore track slip are less commonly used compared to those that consider it, and most of the former are verified only through simulation [4], [32], [33]. Gao et al. [31] verified their algorithm using a micro tracked robot while ignoring the track slippage, but its performance still has room for improvement. Models considering track slip are the mainstream in existing path tracking [3], [12], [19]–[22], [27],

[34]–[36] and parameter estimation [17], [23]–[25] algorithms, with ample real-car verification. The friction-based dynamic model is applied in dynamic control [15], [16], [37]–[43], dynamic analysis [44], [47], [48], parameter estimation [45], [46], and energy management [49]–[51]. Surprisingly, none of the control algorithms for large TRVs that based on friction theory have been verified via real car experiments among the literature surveyed. This might because traditional large TRVs have complex transmission systems, and the torques on both sides are difficult to control; however, it also reflects that the application of the models based on friction theory on large TRVs is limited. Terramechanics-based dynamic models of large TRVs are primarily used in dynamic or possibility analysis [61]. Although most terramechanics-based dynamic models [8], [55] have been verified by real cars, their computational complexity confines their usage to applications insensitive to real-time requirements, such as dynamic analysis.

Therefore, a dynamic model that balances complexity and accuracy is urgently needed for the control of large TRVs, similar to the dynamic models of WVUs using the tire model.

B. Tire Models for WVUs

In the field of WVUs, tire models such as the brush tire model [62], the magic formula [63], and the UniTire model [64] are well-studied and provide significant benefits for the research of WVUs. Tire models can be divided into three types based on their modeling method: physical or theoretical model, empirical model, and semi-empirical model. The brush tire model is a physical model that assumes the tire deformation through the bending of small beams to generate tire force [65]. Empirical models, such as the magic formula, are directly fitted using the tire test data. However, despite their widespread use, physical and empirical models are often criticized for either model accuracy or prediction ability [66]. Semi-empirical models, like the UniTire model [64], combine empirical formulas with theoretical models to achieve better accuracy with fewer parameters. In addition to these models, there are also many other tire models [11], [67], [68]. Moreover, learning-based methods like neural networks have also been employed to describe tire-ground interactions [69]. While the researchers of the WVUs are struggling with selecting the best tire model, researchers in the TRVs field face challenges due to the lack of such an effective model. In this work, we will propose a “tire” model for TRVs and compare it with the UniTire model to demonstrate the similarities between wheels and tracks.

There are also some researchers [11], [70]–[74] apply terramechanics theory to the tire-ground interaction of wheels on soft soil, which demonstrates the compatibility between the theories of TRVs and WVUs. However, most of the works are experimented on soil bins with a rigid wheel [70], [71], [74]. Rigid wheels are seldom used in large vehicles. Taghavifar et al. [11] applied terramechanics theory to real-time control of a wheeled robot in simulation, but the terramechanics theory is only used to calculate the external forces imposed by the deformable soil and use the forces as constants in the dynamic model. Vehicle control in soft soil has always been a challenge, but we look forward to the research progress.

III. MODEL FOR TRVs

The vehicle-ground interaction and its modeling are essential in vehicle dynamics. An efficient and effective vehicle-ground interaction model can enhance vehicle control performance and prevent accidents. In this section, a track-ground interaction model based on terramechanics theory and a slip-aware dual-track dynamic model for TRVs are proposed.

A. The normal pressure-shear displacement relationship

The core of calculating the shear forces lies in knowing the shear displacement of each point on the track, which can then be used to determine the shear stress through the shear displacement-shear stress relationship model. Here, we use the Janosi-Hanamoto's model (Eq. 1) [75] as an example due to its concise form and wide range of applications:

$$\tau = (c + p \tan \varphi) \left(1 - e^{-j/K} \right) \quad (1)$$

where τ is the shear stress, φ is the friction angle. K and j denote the shear deformation parameter and shear displacement, respectively. c and p are the cohesion coefficient and normal pressures, respectively. For non-cohesive soil, we can rewrite the Eq. (1) as

$$\tau = p\mu \left(1 - e^{-j/K} \right) \quad (2)$$

with μ the shear coefficient.

The track-ground pressure changes constantly; thus, we cannot simply integrate the shear velocity as shear displacement is a variable dependent on normal pressure, conforming to the rule (Fig. 2) proposed by Jo Y. Wong [58].

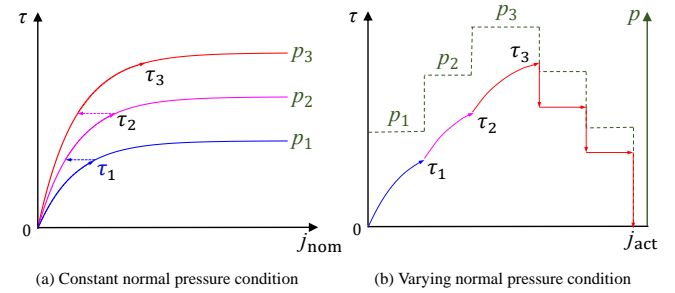


Fig. 2. Shear stress-shear displacement relationship.

When the normal pressure on a track segment increases from 0 to p_3 , the relation between actual shear displacement j_{act} and shear stress τ is illustrated in Fig. 2 (b). However, due to loading changes, we should use the nominal shear displacement j_{nom} rather than the actual displacement j_{act} to calculate the shear stress. The nominal displacement j_{nom} follows the path $O\tau_1\tau_2\tau_3$ as Fig. 2 (a) shows. During the unloading part of the cycle, the shear stress decreases instantaneously with the decrease of normal pressure [58], as shown in Fig. 2 (b). In other words, the higher pressure part contributes more to the nominal displacement and, consequently, more to the

shear stress. The shear displacement transform process can be expressed by:

$$j_b = -K \ln \left(1 - \frac{p_a}{p_b} (1 - e^{-j_a/K}) \right), \quad p_a \leq p_b \quad (3a)$$

$$j_b = j_a, \quad p_a > p_b \quad (3b)$$

where, subscript a and b are used to distinguish different pressure. Assuming the nominal shear displacement at pressure p_a is j_a , the nominal shear displacement should be j_b when the pressure changes to p_b . It should be noted that the Eq. (3) works only on non-cohesive soil in Eq. (2).

B. "Tire model" for TRVs

In this section, a track-ground interaction model is proposed. Inspired by the tire model of WV, the proposed model regards the shear forces below the road wheel as a whole. According to Jo Y. Wong [58], track-ground shear forces can be calculated through integral or summation methods. However, these methods are too complex for model-based real-time control. As mentioned, normal pressure affects shear stress proportionally, and the higher pressure part contributes more to the shear force. Therefore, traditional methods can be simplified by substituting the complex integral or summation with the average states of the high-pressure area.

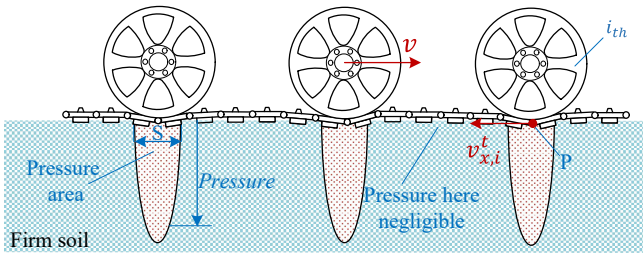


Fig. 3. The track-ground normal pressure on firm soil.

As Fig. 3 shows, the track-ground normal pressure is primarily concentrated in a limited area beneath the road wheels on firm soil. S represents the longitudinal length of the high-pressure area where pressure is not negligible. $v_{x,i}^t$ denotes the longitudinal shear velocity, which can be obtained by Eq.(4). Point P is located on the track directly below the center of the i_{th} road wheel and is also the center of the pressure area. Point P has an average shearing velocity and average shear time of the whole pressure area; thus, point P has the average shearing displacement. Therefore, the states of point P can be used to approximate the states of the entire pressure area. The longitudinal, lateral, and combined shear velocity $v_{x,i}^t$, $v_{y,i}^t$, and v_i^t of point P can be formulated as:

$$v_{x,i}^t = v_{x,i} - rw \quad (4a)$$

$$v_{y,i}^t = v_{y,i} \quad (4b)$$

$$v_i^t = \sqrt{v_{x,i}^{t^2} + v_{y,i}^{t^2}} \quad (4c)$$

where $v_{x,i}$ and $v_{y,i}$ are the velocity of the i^{th} wheel center in longitudinal and lateral directions, and their combined speed

is v_i . r and w represent the sprocket pitch circle radius and speed, respectively. The average shear time t_i^t and average shear displacement j_i can be obtained:

$$t_i^t = \frac{S}{2rw} \quad (5)$$

$$j_i = v_i^t \cdot t_i^t = \frac{S}{2} \sqrt{\left(\frac{v_{y,i}}{rw}\right)^2 + \left(\frac{rw - v_{x,i}}{rw}\right)^2} \quad (6)$$

The longitudinal and lateral slip ratio can be defined as the slip speed over the rolling speed:

$$s_{y,i} = -\frac{v_{y,i}}{rw} \quad (7a)$$

$$s_{x,i} = \frac{rw - v_{x,i}}{rw} \quad (7b)$$

$$j_i = \frac{S}{2} \sqrt{s_{x,i}^2 + s_{y,i}^2} \quad (7c)$$

According to Eq. (2), the track-ground force under a single road wheel can be obtained as

$$F_i = F_z \mu (1 - e^{-Cs_i}) \quad (8a)$$

$$F_{x,i} = \frac{s_{x,i}}{s_i} F_i \quad (8b)$$

$$F_{y,i} = \frac{s_{y,i}}{s_i} F_i \quad (8c)$$

where, $s_i = \sqrt{s_{x,i}^2 + s_{y,i}^2}$, $C = S/(2K)$. It is unnecessary to calculate the exact value of S , as S and shear deformation parameter K will combine to a new parameter C in Eq. (8a), which can be determined experimentally.

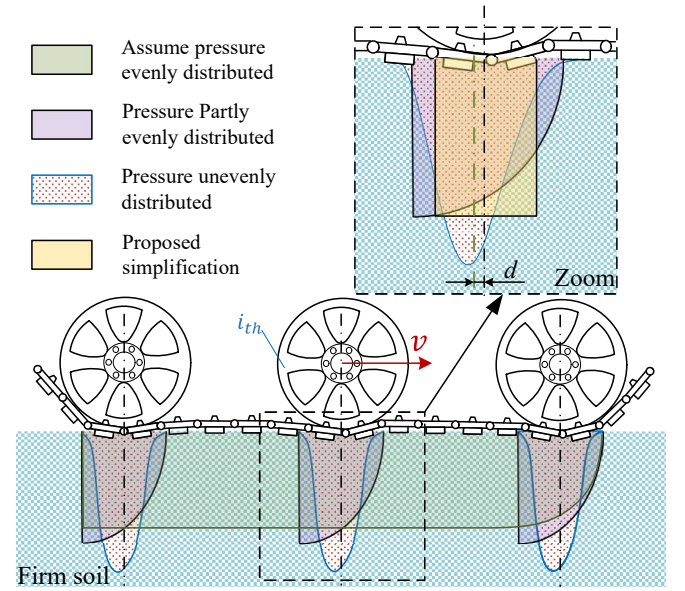


Fig. 4. Shear stress comparison between different methods.

The shear stress is compared to demonstrate the differences between methods, as illustrated in Fig. 4. If the track-ground pressure is assumed to be evenly distributed, the shear stress will increase from front to back until reaching its maximum.

If the track-ground pressure is assumed to be partly evenly distributed, the track-ground stress is concentrated below the road wheel, as shown by the purple area in Fig. 4. However, according to the Jo Y. Wong's theory [58] (Eq. 3), considering the track-ground pressure is not evenly distributed, the track-ground stress should correspond to the dotted area in Fig. 4. In the proposed model, we are no longer focus on the distribution but the effects of the stress. In other words, we care more about the overall force and its direction. As shown in the zoomed part of Fig. 4, we assume that the shear stress, rather than the normal pressure, is evenly distributed, thus avoiding the integral required in other methods. By tuning the width of the high-pressure area S, the overall force can be the same size as the outcome of Jo Y. Wong's theory. Although there is a small distance deviation d between the force center calculated by the two methods, it is negligible in vehicle dynamics.

C. Slip-aware dual-track Dynamic Model

The TRV dynamic model with the longitudinal, lateral, and yaw dynamics in the vehicle body coordinates xoy under a global coordinates XOY is shown in Fig. 5. The TRV turns with a yaw rate γ , an instantaneous rotation center O_s , and an instantaneous rotation radius R . s_0 is the longitudinal distance between O_s and the center of gravity (CoG). φ is the yaw angle between axis x and axis X . b , L and B denote track width, length and center distance, respectively. The origin o_w of the wheel coordinates $x_w o_w y_w$ is at the center of the track-ground pressure area (the shaded area). The resultant ground-track force F_i is in the opposite direction with the shear velocity v_i^t . θ is the angle between axis y_w and v_i^t , where the subscripts i denoted the i^{th} wheel. The ground-track forces in the longitudinal direction F_x always promote the turning process, and the corresponding influence results in a driving moment M_t . Similarly, $F_{y,i}$ constantly impedes turning, which results in a resistance moment M_r .

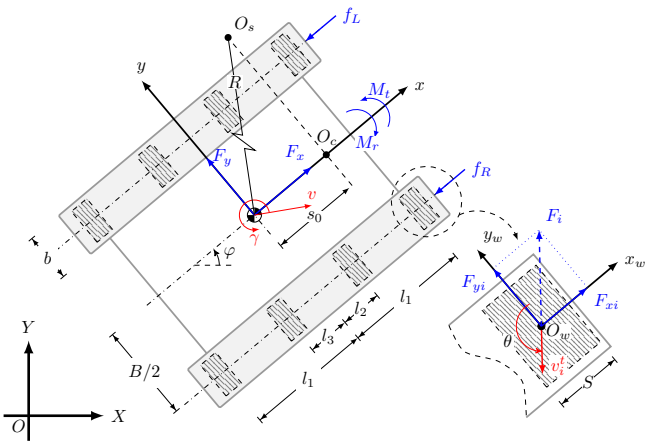


Fig. 5. Dual-track Dynamic Model.

Based on Newton's law of motion, the dual-track dynamic model for dynamic motion control can be formulated as:

$$\dot{v}_x = v_y \gamma + \frac{1}{m} \sum_{i=1}^n (F_{x,i}^R + F_{x,i}^L) \quad (9a)$$

$$\dot{v}_y = -v_x \gamma + \frac{1}{m} \sum_{i=1}^n (F_{y,i}^R + F_{y,i}^L) \quad (9b)$$

$$\dot{\gamma} = \frac{1}{I_z} \left[\frac{B}{2} (F_x^R - F_x^L) - \sum_{i=1}^n (l_i F_{y,i}^R + l_i F_{y,i}^L) \right] \quad (9c)$$

where, $F_{x,i}$ and $F_{y,i}$ are longitudinal and lateral track-ground forces of the i^{th} wheel, which can be calculated by Eqs (7)-(8). I_z is moment of inertia. Turning resistance moment $M_t = \sum_{i=1}^n (l_i F_{y,i}^R + l_i F_{y,i}^L)$.

Based on the above theories, TRVs can be treated as particular skid-steer WV with the following properties:

- a) The TRV on firm ground can be considered as a particular skid-steer WV with the same number of wheels as its road wheels;
- b) The “wheels” on one side have the same rotational speed, and the same slip ratio;
- c) Ground-track forces in the longitudinal direction drive the vehicle to turn, while forces in the lateral direction impede the turning;
- d) The interaction between the “Wheels” and the ground is assumed to be isotropic;
- e) The driving forces of wheels on the same side could meet the demand adaptively.

IV. COMPARISON WITH THE UNITIRE MODEL

People have been emphasizing the difference between TRVs and WV as if they are two totally different things, but both of them are vehicles on the ground. In this section, we will compare the UniTire model [76] of WV and the proposed “tire” model of TRVs to reveal the underlying relationship of these two different types of vehicles.

A. Comparison in forms

As shown in Table II, the proposed “tire” model for TRVs is similar in the overall form to the UniTire model of WV, despite being derived from different theories. This similarity indicates a commonality exists in the vehicle-ground interaction, which will be discussed in detail in Section IV-C. Here, we focus on the three differences in their forms to better understand the essence of vehicle-ground interaction.

The first difference is that the model of TRV is isotropic, while the model of WV is anisotropic, as manifested in the parameters K and μ . In the TRV model, parameters K and μ are inherent parameters of soil called the shear deformation parameter and the shear coefficient, respectively. They remain constant as long as the soil's state is unchanged. In contrast, the longitudinal slip stiffness K_x and cornering stiffness K_y in the WV model are related to normal load F_z and friction coefficients μ_x and μ_y . Additionally, a modification factor λ is introduced to help to deal with the anisotropy [64]. The tire structure causes the anisotropy: typically a rubber tread for road contact, metal belts for strength and stability, and

TABLE II
COMPARISON BETWEEN THE PROPOSED MODEL AND THE UNiTIRE MODEL.

| Proposed Model ¹ | UniTire model ¹ |
|---|---|
| $F_x = \frac{\sigma_x}{\sigma} F_z \mu (1 - e^{-\kappa})$ | $F_x = \frac{\sigma_x}{\sigma} F_z \mu_x (1 - e^{-\kappa})$ |
| $F_y = \frac{\sigma_y}{\sigma} F_z \mu (1 - e^{-\kappa})$ | $F_y = \frac{\sigma_y}{\sigma} F_z \mu_y (1 - e^{-\kappa})$ |
| where, | |
| $\sigma_x = K \frac{(rw - v_x)}{rw}$ | $\sigma_x = \frac{\lambda K_x}{F_z \mu_x} \frac{(rw - v_x)}{rw}$ |
| $\sigma_y = K \frac{v_y}{rw}$ | $\sigma_y = \frac{K_y}{F_z \mu_y} \frac{v_y}{rw}$ |
| $\sigma = \sqrt{\sigma_x^2 + \sigma_y^2}$ | $\sigma = \sqrt{\sigma_x^2 + \sigma_y^2}$ |
| $\kappa = -\sigma$ | $\kappa = -\sigma - E_1 \sigma^2 - (E_1^2 + \frac{1}{12}) \sigma^3$ |
| $\mu = \text{constant}$ | $\mu = \mu_s + (\mu_m - \mu_s) e^{\Pi}$ |
| $\lambda = 1$ | $\Pi = -\mu_h^2 \lg^2 \left(\left \frac{v_s}{v_{sm}} \right + Ne^{-\left \frac{v_s}{v_{sm}} \right } \right)$ |

¹ To make the comparison intuitive, the notations are slightly different from the articles.

sidewalls for lateral support. If we assume the tire to be isotropic, that is, $K_x = K_y$ and $\mu_x = \mu_y$, and replace $\frac{\lambda K_x}{F_z \mu_x}$ and $\frac{K_y}{F_z \mu_y}$ with a unified K , the two models exhibit the same basic form.

The second difference is that the parameter κ in TRVs is the same as κ in WV, except for the higher-order terms σ^2 and σ^3 . The term σ shown in Table II is related to but not identical to the slip ratio. Since σ is generally small, the higher-order terms have a limited effect on the overall performance of the proposed model. Whether to include higher-order terms to the proposed TRV model needs to be determined by precise experimental equipment and detailed tests. Given the limitations of current experimental equipment and the limited impact of the high-order terms, we will not focus on these terms for the time being.

The third difference is that the shear coefficient μ in TRVs is a constant, whereas the friction coefficient μ in WV varies with the slip velocity v_s due to the property of rubber [77], [78]. Such properties are not found in soil, and existing studies [79], [80] generally agree that the effect of shear velocity on soil strength of the non-cohesive soil is limited. In addition, it should be clear that in the field of TRVs the relative motion between tracks and soil is called shear, whereas in the field of WV the relative motion between wheels and ground is called slip. While shear and slip are different by definition, they exhibit similar mechanical properties.

In conclusion, most differences arise from the unique structure of the inflated tire, such as the anisotropy and rubber slip properties. If we assume the tire is isotropic and neglect the higher-order terms in κ and the unique property of rubber, the UniTire model is the same as the proposed model in form.

B. Comparison in model outputs and applications

The relationship between slip ratio and the ground forces in TRVs and WV are similar, but the trend is achieved in

different methods. As shown in Fig. 6, the hump is existing in both the UniTire model and the proposed “tire” model using the Bekker’s shear displacement-shear stress model.

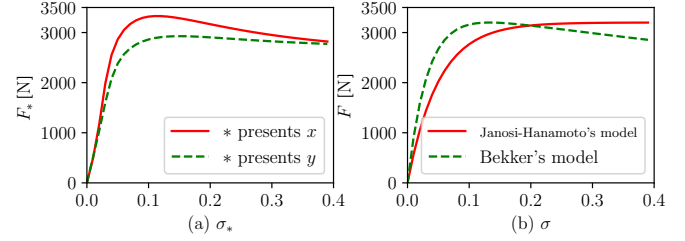


Fig. 6. Model comparison in outputs. (a) The Unitire model in longitudinal and lateral direction; (b) The comparison of the “tire” model using the Janosi-Hanamoto’s model and the Bekker’s model.

The Bekker’s model [79] is as following:

$$\tau = \frac{c + p \tan \varphi}{y_{\max}} \left[e^{(-K_2 + \sqrt{K_2^2 - 1}) K_1 j} - e^{(-K_2 - \sqrt{K_2^2 - 1}) K_1 j} \right] \quad (10)$$

where, K_1 and K_2 are slip parameters, and y_{\max} is the maximum value in the square brackets. In the terramechanics theory, the hump is caused by the brittleness of the soil and is related to the shear displacement j or the slip ratio s . Janosi-Hanamoto’s model is concise, but it cannot depict the hump. The UniTire model is similar to the proposed “tire” model using Janosi-Hanamoto’s model in forms, but Savkoor’s formula [77], [78] is employed to allow the friction coefficient μ changes with the slip velocity enabling the model to exhibit a hump of maximum tire force. Similar techniques could potentially be used to expand the application of the Janosi-Hanamoto’s model.

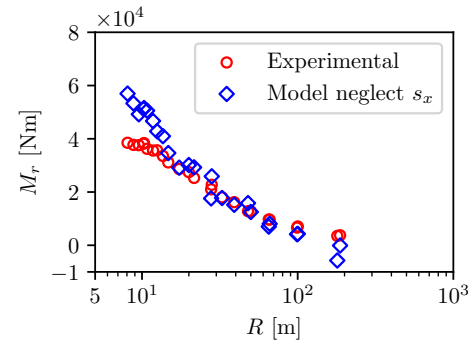


Fig. 7. Effects of the TRV longitudinal slip on model performance.

The applications of the models are not the same due to the distinct turning mechanisms of TRVs and WV. WV turn by changing the wheels’ direction, and the longitudinal slip is negligible. Therefore, the influence of the longitudinal slip can generally be ignored, and the lateral dynamics can be linearized at the zero point, making the tire model a linear model as long as the slip angle is limited. However, the longitudinal and the lateral dynamics of TRVs are strongly coupled. As Fig. 1 (c) illustrates, during the turning process, lateral forces will result in a turning resistance moment impeding the TRV from turning. The longitudinal force is required to provide a turning drive moment to maintain the turn. In other words, the lateral

forces constantly impede turning, but the longitudinal forces always drive the turning. The smaller the turning radius, the larger the lateral and longitudinal slips. Thus, the lateral and longitudinal slips of TRVs have similar trends and magnitudes. Unlike WV, we cannot neglect the slip in one direction when estimate the state in the other direction. Experimental results also support our opinion. As Fig. 7 shows, neglecting the longitudinal slip will cause non-negligible model errors, especially in a small turning radius.

C. Similarity in mechanisms

We have discussed the similarity in phenomena such as model forms, outputs, and applications, but the underlying mechanisms still need to be explored. Vehicle-ground interaction models essentially establish a mapping relationship between relative motion and forces. When considering a soft and a hard object rubbing against each other, the best way to establish the motion-stress relationship is to focus on the soft object, as its deformation is more accessible to measure. For TRVs, the soil is the soft object; however, for WV, the tires are softer compared to road. Thus, we study the track-ground interaction in terramechanics, and the tire-ground interaction in tire dynamics. Fig. 8 compares the tire deformation of WV and the ground deformation under front road wheel of TRV in elevation views and plan views, respectively. The deformation in tire-ground interaction mainly occurs in the tire, while the deformation of the track-ground interaction occurs in the soil. Both interactions represent the frictional relationship between soft and firm objects. Therefore, the tire-ground and track-ground interaction mechanisms are similar, reflecting the interaction between rolling and stationary objects with different stiffness, although we use the term “slip” in WV but “shear” in TRVs.

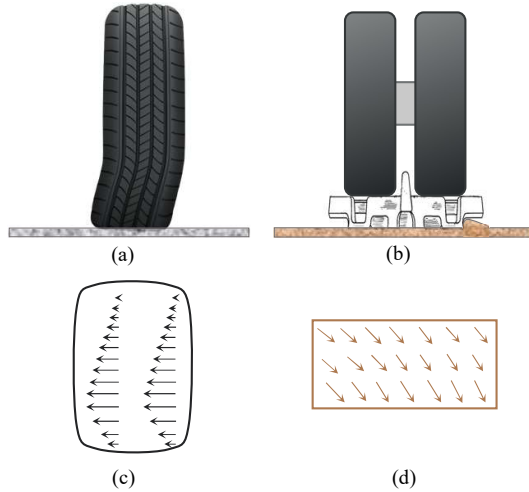


Fig. 8. Comparison of (a) the tire deformation and (b) the ground deformation under front road wheel of TRV in back view, (c) the tire deformation of contact patch relative to vehicle body and (d) the ground deformation of contact patch relative to ground when vehicle moving inward and right turn.

The interaction mechanism of tracks and tires is similar, but why does the similar mechanism lead to different interaction models? The core difference between the proposed

“tire model” and the UniTire model is the anisotropy/isotropy. The anisotropy of the tire is evident in two aspects: the friction coefficients and the tire stiffness. In other words, the friction circle is an ellipse, and the stiffness varies with direction. However, the exponential part ($1 - e^{-x}$) in the stress-displacement empirical model in Table II can not be used directly in anisotropy situations. Therefore, normalization should be employed to enable the application of the stress-displacement empirical model, with $\frac{K_x}{F_z \mu_x}$ together with $\frac{K_y}{F_z \mu_y}$ as the coefficients to normalize the longitudinal and lateral slip ratios. In addition, the anisotropy makes the direction of the tire force difficult to estimate. The directions of shear stress in the adhesion region and the sliding region of the contact patch are not the same [64]. When the slip is slight, $\frac{F_x}{F_y} \approx \frac{K_x S_x}{K_y S_y}$; however, for a large slip condition $\frac{F_x}{F_y} \approx \frac{S_x}{S_y}$. Thus, the modification parameter λ in Table II is introduced to enable the direction of the tire force to gradually change from the direction of the adhesion region to the slip region as the slip increases. Therefore, it is the different manifestations of similar mechanisms on tracks and tires that lead to different forms of models.

In conclusion, the tire-ground and the track-ground interactions share similar mechanisms, although they have developed into different theories. The core difference between tires and tracks is that the pneumatic rubber tires are anisotropic, but the steel tracks are not.

V. EXPERIMENTAL RESULTS AND ANALYSIS

A. Experimental setup

The proposed “tire” model is verified and validated via an autonomous forest fire rescue TRV, as shown in Fig. 9 (a). The test TRV is driven by motors on both sides, and the transmission system on one side is shown in Fig. 9 (b). The drive motors provide real-time feedback on torques and speeds, allowing the calculation of driving forces and track winding speed via the gear ratio. As Fig. 9 shown, the test TRV is equipped with the differential global positioning system (GPS) and inertial measurement unit (IMU), which collect the pose and motion information of the vehicle. The IMU is positioned near the driver’s position, approximately 0.85 meters forward of the vehicle’s geometric center. The GPS antenna is mounted on the car shell above the IMU. The parameters of the test TRV and field are listed in Table III. One of the primary purposes of proposing a “tire” model for TRVs is to fill the research gaps that we don’t have a ready-made, efficient, and effective dynamic model for motion control of TRVs. Therefore, we verified the proposed model with the whole dynamic of the test vehicle. Verifying with the whole dynamic is closer to actual motion control tasks and does not require special equipment. Similar to previous works [8], [63], the values of the soil parameters are determined by fitting the data.

The tire model focuses on the characteristics of the tire, but the track-ground interaction model emphasizes the properties of the ground. Thus, the proposed model is verified on different types of soil with different compaction and properties, including sand-gravel road and sand-dirt road. The overall verification process is divided into three parts. Firstly, we have

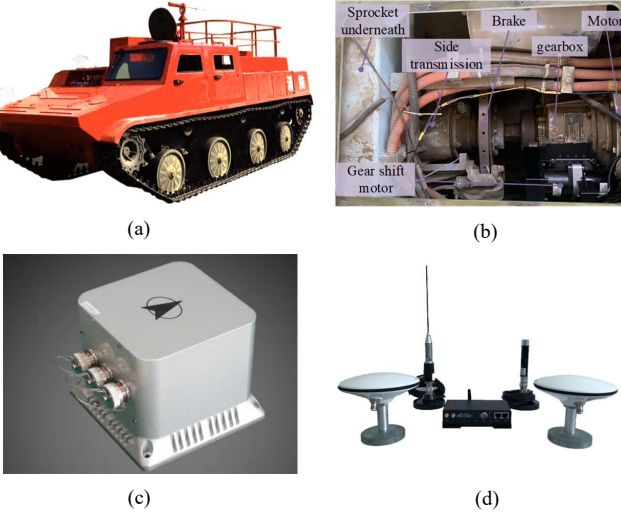


Fig. 9. The test vehicle and its equipment. (a) the test vehicle, (b) the transmission system on the left side, (c) IMU, (d) GPS.

measured the ground pressure to demonstrate the track-ground pressure is mainly concentrated below the road wheels on firm ground rather than being evenly distributed. The concentrated pressure is a crucial prerequisite for model derivation. Secondly, the steady-state performance of the proposed model is verified. Vehicles are subject to random excitation, such as road irregularity while driving, and using steady-state data helps reduce the effects of these noises. Thirdly, we also demonstrate the effectiveness of the proposed model in the non-steady-state conditions. Generally, terramechanics-based methods are primarily used in steady state [8], [55] due to the model complexity, but the proposed model could handle non-steady-state scenarios easily. In the last, a total of over 500 groups of data are collected and used to verify the proposed model.

TABLE III
PARAMETERS USED IN THE VERIFICATION.

| Parameter | Value/unit | Description |
|-------------|---------------------|---|
| m | 9660kg | Vehicle mass |
| B | 2.464m | Track center distance |
| b | 0.365m | Track width |
| L | 2.703m | Track-ground contact length |
| r | 0.2654m | Sprocket pitch circle radius |
| n | 4 | Number of road wheel in single side |
| T_{err} | $\leq 10\text{Nm}$ | Torque feedback error |
| P_{err} | $\leq 15\text{cm}$ | GPS positioning error |
| I_z | 15800kgm^2 | Moment of inertia |
| C | 16 | Parameter in proposed model |
| μ | 0.7 and 0.75 | Shear coefficient on gravel and dirt road |
| μ_{max} | 0.77 | Parameter used in Nikitin formula |
| a | 0.89 | Parameter in Nikitin formula |

The proposed model is triple-verified by longitudinal, lateral, and yaw dynamics in the model verification process. Since only the longitudinal force can be measured directly through motor torque feedback, the lateral and yaw dynamics are verified indirectly by the full dynamic model in Eq. (9). The measured sprocket forces \hat{F}_s^* , lateral force \hat{F}_y and turning

resistance moment \hat{M}_t are obtained using Eq. (11), where the superscript * denotes L or R .

$$\hat{F}_s^* = \frac{T^*}{r} \quad (11a)$$

$$\hat{F}_y = m\dot{v}_y + mv_x\gamma \quad (11b)$$

$$\hat{M}_t = \frac{B(T^R - T^L)}{2r} - I_z\dot{\gamma} \quad (11c)$$

where, T^* and r are the torque output and pitch circle radius of the sprocket, respectively. T^* is obtained by motor feedback. The linear and yaw velocities are obtained by integrating the linear and yaw accelerations collected by the IMU. For steady-state turning, the lateral acceleration \dot{v}_y and yaw acceleration $\dot{\gamma}$ are assumed to be zero.

The estimated sprocket forces \hat{F}_s^* , lateral force \hat{F}_y and turning resistance moment \hat{M}_t are obtained by Eq. (12).

$$\hat{F}_s^* = \sum_{i=1}^n F_{x,i}^* + f \quad (12a)$$

$$\hat{F}_y = \sum_{i=1}^n (F_{y,i}^R + F_{y,i}^L) \quad (12b)$$

$$\hat{M}_t = \sum_{i=1}^n (l_i F_{y,i}^R + l_i F_{y,i}^L) \quad (12c)$$

where, f represents the rolling resistance of the track. The ground-track forces below the i^{th} wheel on both sides, $F_{x,i}^*$ and $F_{y,i}^*$, are estimated via Eq. (8). The inputs are each wheel's longitudinal and lateral slip ratio, which are calculated by the yaw rate, velocity, and sprocket speeds on both sides.

B. Model verification on sand-gravel road

The experiment on the sand-gravel road was conducted in June 2021 at a farmland area around $37^{\circ}50'17.3''\text{N}$ and $114^{\circ}23'22.6''\text{E}$ in Shijiazhuang, Hebei Province, China. The weather was sunny during the collection, with no precipitation in the last ten days. The test site is shown in Fig. 10 (a), and its physical properties are presented in Fig. 10 (b). Its upper layer is dry and loose, while the lower layer is firm. We can see fine sand mixed with stones and plant residue on its upper layer. The track-ground pressure was measured by a pressure sensor, as Fig. 10 (c) shows. The sensor is buried approximately 5 cm deep in the soil to allow the test TRV to run over at a constant speed [81]. The time series of the pressure signal was collected via an electronic control unit and converted into a spatial series based on the constant velocity. According to the literature [82], a depth of 5 cm has a limited impact on measure accuracy for a TRV with a track width of 36.5 cm. The experimental result is qualitative because we have replaced a key resistor in the amplifier with a non-precision one to meet the range requirements. Our focus was on the distribution rather than the value of the pressure. The experimental result qualitatively demonstrates that the track-ground pressure is mainly concentrated in a limited area below the road wheel in a multi-peak form, as shown in 10 (e), which supports the track-ground pressure suppose.

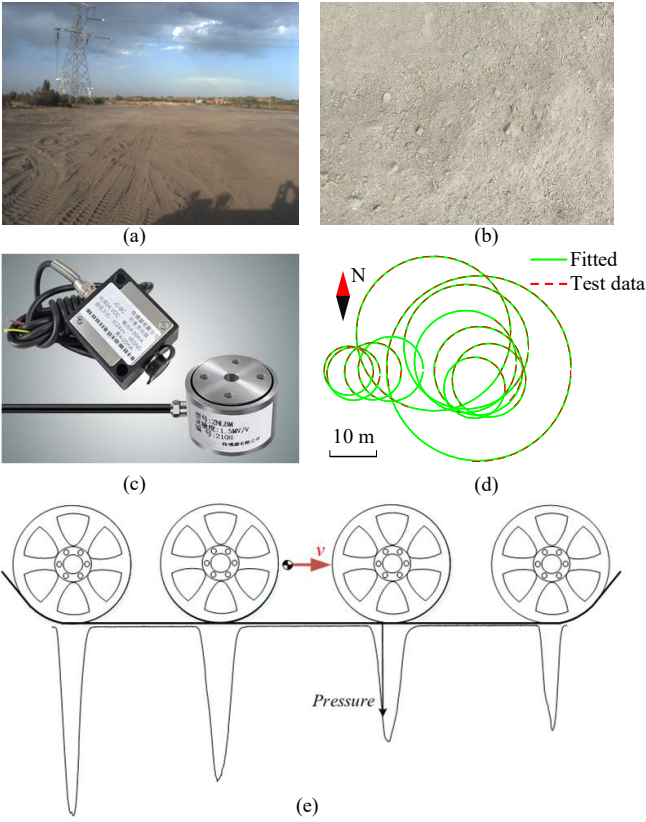


Fig. 10. The sand-gravel test site introduction. (a) The test site, (b) soil details, (c) the pressure sensor, (d) position data and fitted circles, (e) track-ground pressure.

The steady state data of the test TRV is collected with the following procedure. Firstly, a series of fixed speed instructions were sent to and executed by the motor controllers on both sides while collecting data from IMU, GPS, and vehicle control unit (VCU). Then, the collected data is cropped manually. Position data is fitted with circles as Fig. 10 (d) shows, allowing us to precisely determine the turning radius. Finally, the data is compared with the estimated data at different velocities and directions, as shown in Fig. 11. Both the left turn and right turn are compared to mitigate the influence of track tension.

The proposed model is verified with the dynamic response of a real TRV on general soil ground rather than precise lab data. Although it is closer to the actual application of the model, it introduces more measurement errors. Additionally, the slip ratio significantly impacts the ground-track force estimation. However, the model outputs show good consistency with the measured results in trends in most scenarios, as shown in Fig. 11. Two points need explanation. Firstly, when vehicle speed is low, the consistency is not as good as that at high speed. There are two main reasons for this. On the one hand, lower vehicle speed means lower track-ground slip velocity, which increases the measured percentage error. On the other hand, the model input of the measured velocity should be the velocity of the unsprung part; however, our IMU is mounted on the body, and the body acceleration is more affected by road excitation. Compared with low speed, lateral force is larger

at high speed. A larger lateral force will suppress vehicle suspension, and the body acceleration will be more stable to make the measured velocity is more accurate. However, 3 kilometers per hour is slower than a human walk. Thus, we are not surprised by the poor performance at 3 km/h. Secondly, the estimated lateral force seems more dispersed. The lateral velocity is obtained by integrating the acceleration, but the vehicle body is subject to roll oscillation. Since the lateral velocity is generally small, even slight oscillation impacts the lateral velocity. In addition, the integrating process also introduces errors. As shown in Fig. 11 (d)-(f) and (j)-(l), the estimated longitudinal forces on both sides deviate from the measured value together. The error of the integration obtained longitudinal velocity caused the deviation.

In the motion control of TRVs, the yaw dynamic is the most important and irreplaceable aspect. Compared with the longitudinal and lateral forces, turning resistance moment M_t is less affected by body swing for yaw rate data of IMU is robust to body vibration and roll. As Fig. 12 shows, the model performance on M_t is better than that on F_x and F_y because M_t is less affected by the unstable v_y . Figs 12 (a)-(c) estimate M_t with v_y obtained by integration, but Figs 12 (d)-(f) assume $v_y = 0$. The results indicate that neglecting the v_y even improved the model performance at low speed because v_y is small but introduces large errors. However, at high speed, v_y is not negligible. Therefore, when the turning radius is small, estimation results considering v_y at 15 km/h performs better than that do not. The mean absolute error (MAE) and the coefficient of determination R^2 of the turning resistance moment are compared in Table IV. The MAE value of M_t considering v_y improves with the speed increase, as the measured percentage error decreases with the speed increase. Conversely, the MAE value assuming $v_y = 0$ deteriorates with the increasing speed, because the impacts of the lateral velocity are not negligible with the required lateral force F_y increase. Similar trends are observed in the comparison of R^2 .

TABLE IV
THE MAE AND R^2 COMPARISON OF M_t ON SAND-GRAVEL ROAD.

| Indicator | Model | 3km/h | 10km/h | 15km/h |
|-----------|----------------|-------|--------|--------|
| MAE | consider v_y | 2522 | 2360 | 1469 |
| | let $v_y = 0$ | 804 | 1116 | 1618 |
| R^2 | consider v_y | 0.931 | 0.967 | 0.979 |
| | let $v_y = 0$ | 0.996 | 0.992 | 0.975 |

Fig. 13 shows the model performance during real-time non-steady lane change maneuvers at different velocities. As depicted in Fig. 13 (a), the continuous lane change maneuver is achieved by varying the track velocities n on both sides. s_x represents the longitudinal slip, which is directly related to the longitudinal and lateral ground force F_x and F_y as Eq. (7)-(9) shown. There is good consistency in the trend, further proving the validity of the proposed model. However, a similar problem to steady-state verification arises. The sensors are mounted on the sprung part, which experiences larger swing amplitudes during cornering or roll. Consequently, overshoot can be observed in estimated F_x and F_y , especially in the

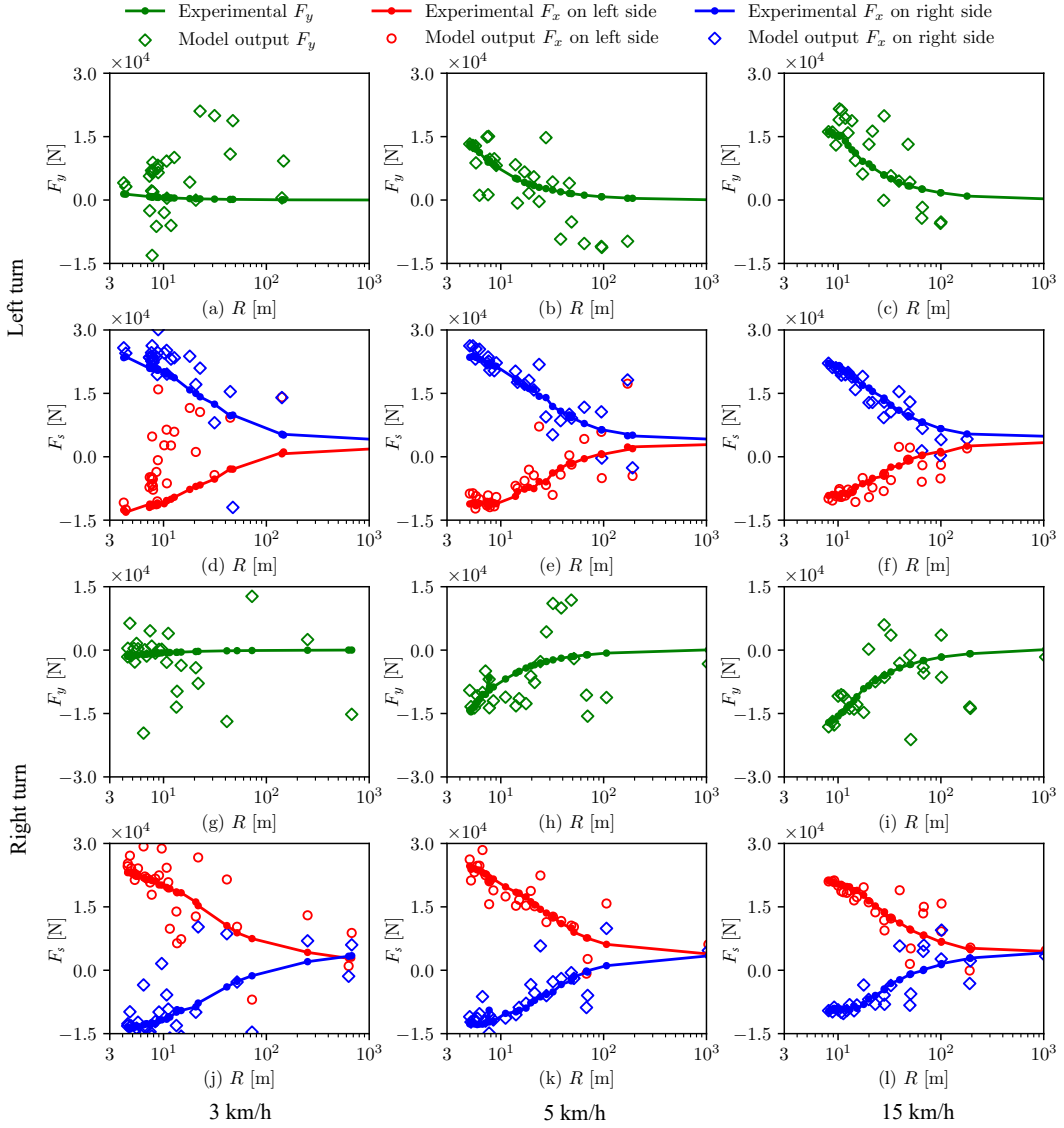


Fig. 11. Steady-state model verification when left turn and right turn at different velocities.

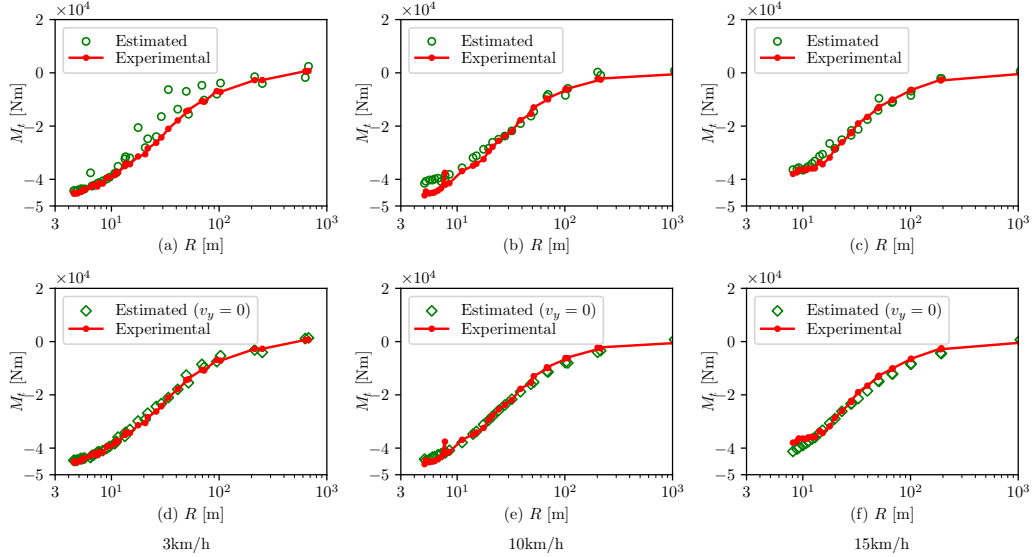


Fig. 12. Turning resistance moment estimation when right turn at (a) 3km/h, (b) 10km/h, (c) 15km/h and estimation neglecting v_y at (d) 3km/h, (e) 10km/h, (f) 15km/h.

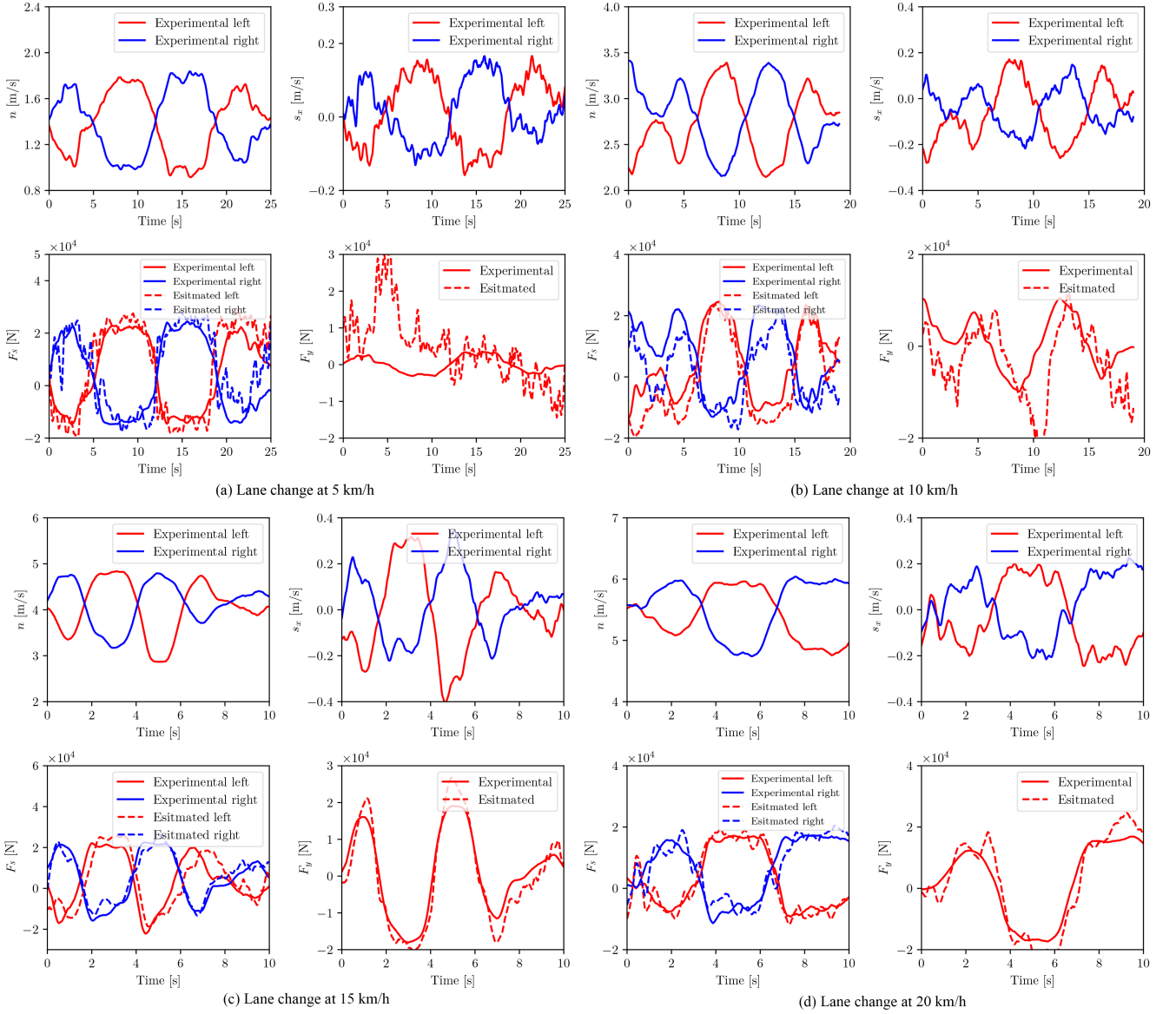


Fig. 13. Continuous lane change maneuver at (a) 5 km/h, (b) 10 km/h, (c) 15 km/h and (d) 20 km/h

lateral direction. This is because the stiffness in the pitch direction is larger than in the roll direction.

C. Model verification on sand-dirt road

The experiment on sand-dirt road was conducted as a supplement of road types in August 2023, at a farmland area around $40^{\circ}17'14.37''\text{N}$ and $115^{\circ}41'48.42''\text{E}$ in Zhangjiakou, Hebei Province, China. Light precipitation happened during the collection. Data at 3 km/h was collected before it rained, and the soil is shown in Fig. 14 (a). The rest of the data was collected after it rained, and the soil is presented in Fig. 14 (b). Fig. 14 (c) shows the turning maneuver and track prints. The scratches are mainly concentrated on both sides of the track prints in Fig. 14 (d). The lower and upper scratches are caused by the 3rd and 4th road wheel respectively, proving that the track ground pressure is concentrated under the road wheels. Only steady state data is collected on sandy-dirt road.

Fig. 15 shows the comparison of the turning resistance moment M_t on the sand-dirt road at different velocities. The model performance at 3 km/h is not as good as that at 5 km/h and 10 km/h because the rain altered the soil properties, yet the same model parameters are used for the whole estimation. This demonstrates that soil properties are closely related to environmental factors such as moisture content [83]. Despite the soil is softer than sand-gravel soil, the model still performs well, as Fig. 15 (b) and (c) show. As Fig. 15 (d) shows, the M_t at different speeds is basically the same when the speed is low.

Existing dynamic models of TRVs for motion control are primarily friction-based dynamic models. The difference between the Coulomb's law of friction-based model, the Nikitin empirical formula-based model, and the Janosi-Hanamoto model is shown in Fig. 16. The Coulomb's law of friction can be treated as a particular case of the Janosi-Hanamoto model

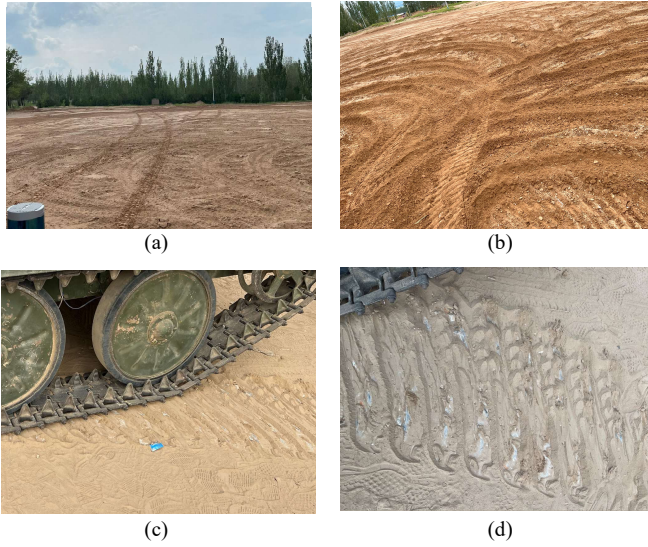


Fig. 14. Test site introduction of which (a) Soil before rain, (b) soil after rain, (c) turning maneuver and (d) track prints.

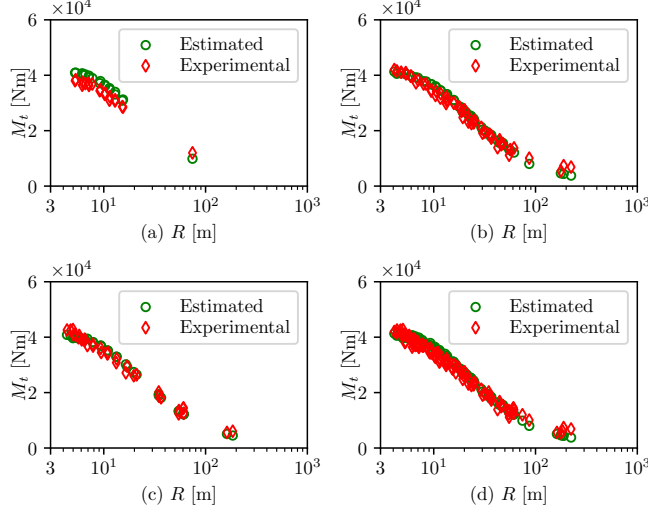


Fig. 15. Turning resistance moment comparison on sand-dirt road at (a) 3 km/h, (b) 5 km/h, (c) 10 km/h and (d) 3-10 km/h.

when the shear deformation parameter K is zero or infinitely close to zero. The Nikitin empirical formula-based model assumes the friction coefficient μ' changes as the turning radius changes, as shown in Eq. (13).

$$\mu' = \frac{\mu_{\max}}{a + (1-a)\frac{R+B/2}{B}} \quad (13a)$$

$$M_t = \frac{1}{4} GL\mu' \quad (13b)$$

where, a is a parameter, and $a = 0.85$ is recommended. μ_{\max} is the friction coefficient when the turning radius is $B/2$. G denotes the weight. The Nikitin empirical formula is designed for estimating the turning resistance moment M_t with Eq. (13b), where the turning center O_c in Fig. 5 is assumed located on the center of the vehicle. That is, ignore the lateral

dynamics. Consequently, the Nikitin empirical formula cannot estimate lateral and longitudinal track-ground forces.

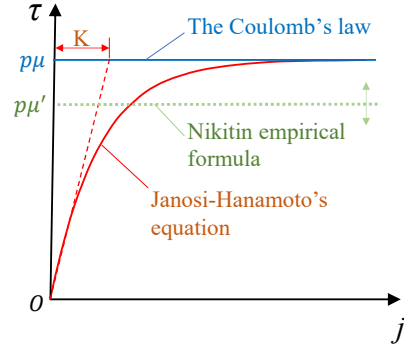


Fig. 16. The difference between the Coulomb's law-based model, the Nikitin empirical formula-based model and the Janosi-Hanamoto model.

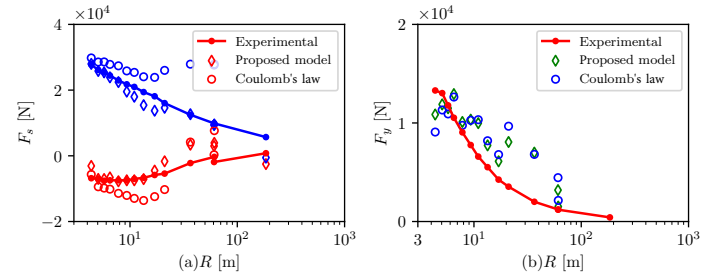


Fig. 17. The longitudinal and lateral performance comparison on sand-dirt road at 10 km/h and left turn.

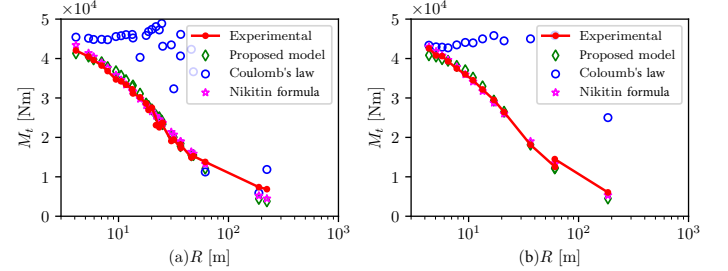


Fig. 18. The turning resistance moment performance comparison on sand-dirt road left turn at (a) 5 km/h and (b) 10 km/h.

The longitudinal and lateral performance of the models is compared in Fig. 17. The parameters were obtained by fitting the experimental data for optimal performance. Due to its limitation, the Nikitin formula-based model is not shown in Fig. 17. The Coulomb's law-based model is employed by assuming K is near zero. As shown, the Coulomb's law-based model overestimates the magnitude of the longitudinal forces because it neglects the shear displacement-shear stress relationship. However, the proposed model fits the experimental data well. A similar phenomenon is observed for the turning resistance moment in Fig. 18. The Nikitin formula-based model performs comparably to the proposed model. The MAE and the coefficient of determination R^2 of the turning resistance moment are compared in Table V. The performance

of the Nikitin formula-based model is slightly better than the proposed model. However, the Nikitin formula is an empirical model and can only be used to estimate the turning resistance moment. The Coulomb's law-based model performed poorly in the experiments, but this does not mean the model is wrong. In fact, the Coulomb's law-based model may be applicable to tracked robots on cement roads or indoor hard ground.

TABLE V
THE MAE AND R^2 COMPARISON OF M_t ON SAND-DIRT ROAD.

| Velocity | Proposed model | | Nikitin model | | Coulomb model | |
|----------|----------------|-------|---------------|-------|---------------|--------|
| | MAE | R^2 | MAE | R^2 | MAE | R^2 |
| 5 km/h | 1133 | 0.978 | 1002 | 0.984 | 14777 | -2.019 |
| 10 km/h | 759 | 0.992 | 556 | 0.996 | 13573 | -1.235 |

VI. CONCLUSION

TRVs and WVVs have developed independently in parallel, and little work has revealed the underlying mechanisms of the vehicle-ground interaction. In this work, a “tire” model for TRVs is proposed to fill the research gap in the lack of an efficient and effective dynamic model for motion control of TRVs. A detailed comparison between the proposed “tire model” and the UniTire model demonstrates that the differences between the two models are simply different manifestations of similar mechanisms on various materials. Finally, detailed real TRV experiments were conducted to verify the proposed “tire” model.

The contribution of this work is multi-faceted. Firstly, due to the model complexity, traditional terramechanics-based methods were mainly used in steady-state turning maneuvers [8], [55] or multibody dynamics simulation. The proposed “tire” model enables terramechanics-based methods to be applied in real-time motion control of TRVs. A substantial amount of experimental data on different soils, velocities, and scenarios proves the model’s effectiveness. Secondly, knowing the underlying mechanisms behind the vehicle-ground interaction will benefit both TRVs and WVVs. The relationship between TRVs and WVVs can help apply theories, methods and techniques of WVVs like ABS and ESP to the TRV field. For WVVs, we generally assume the ground is firm, and the deformation occurs in the tires. However, on some unpaved roads, both soil and tires may deform together. Thus, learning from TRVs could help improve the theory and expand the application of tire models.

Although experiments have proven the effectiveness of the proposed model, there is still room for improvement. The proposed model is verified with the whole dynamic of the test vehicle, which is closer to the motion control task while no special equipment is required. However, the onboard sensors are not as accurate as lab equipment, which limits the precise adjustment of the model. Moreover, in the model derivation, the track-ground pressure is assumed to be concentrated in a limited area. That is, the proposed model only works on **firm** ground, but how firm is firm? The application boundaries of the proposed model still need further study with precision equipment on various soil types.

APPENDIX PROPOSED DYNAMIC MODEL OF TRVs

A summary is made of the proposed model. The soil is assumed to be non-cohesive and firm. The “tire model” of the TRV is shown in Eq. (14) and (15).

$$s_{y,i} = -\frac{v_{y,i}}{rw} \quad (14a)$$

$$s_{x,i} = \frac{rw - v_{x,i}}{rw} \quad (14b)$$

$$s_i = \sqrt{s_{x,i}^2 + s_{y,i}^2} \quad (14c)$$

$$F_i = f(s_i) \quad (15a)$$

$$F_{x,i} = \frac{s_{x,i}}{s_i} F_i \quad (15b)$$

$$F_{y,i} = \frac{s_{y,i}}{s_i} F_i \quad (15c)$$

where, $f(s_i)$ depends on the soil type. Eq. (16a) is for plastic soil which do not exhibit a ‘hump’, like sand; therefore, the Janosi-Hanamoto’s model [75] is applicable. For soils that exhibit the ‘hump’, Eq. (16b) is recommended based on the Bekker’s theory [79]. Although the proposed model provides an open interface for different terramechanics equations, only the Janosi-Hanamoto’s model is used as an example and verified in this work for the sandy test soil.

$$f(s_i) = F_z \mu (1 - e^{-Cs_i}) \quad (16a)$$

$$f(s_i) = \frac{F_z \mu}{y_{\max}} \left[e^{(-K_2 + \sqrt{K_2^2 - 1})Cs_i} - e^{(-K_2 - \sqrt{K_2^2 - 1})Cs_i} \right] \quad (16b)$$

where, $C = S/(2K)$ in Eq. (16a), and $C = SK_1/2$ in Eq. (16b). The proposed “tire model” of the TRV is verified by the full dynamic model of the TRV in Eq. (17).

$$\dot{v}_x = v_y \gamma + \frac{1}{m} \sum_{i=1}^n (F_{x,i}^R + F_{x,i}^L) \quad (17a)$$

$$\dot{v}_y = -v_x \gamma + \frac{1}{m} \sum_{i=1}^n (F_{y,i}^R + F_{y,i}^L) \quad (17b)$$

$$\dot{\gamma} = \frac{1}{I_z} \left[\frac{B}{2} (F_x^R - F_x^L) - \sum_{i=1}^n (l_i F_{y,i}^R + l_i F_{y,i}^L) \right] \quad (17c)$$

REFERENCES

- [1] N. Guo, B. Lenzo, X. Zhang, Y. Zou, R. Zhai, and T. Zhang, “A real-time nonlinear model predictive controller for yaw motion optimization of distributed drive electric vehicles,” *IEEE Transactions on Vehicular Technology*, vol. 69, no. 5, pp. 4935–4946, 2020.
- [2] H. Zhou, F. Jia, H. Jing, Z. Liu, and L. Güvenç, “Coordinated longitudinal and lateral motion control for four wheel independent motor-drive electric vehicle,” *IEEE Transactions on Vehicular Technology*, vol. 67, no. 5, pp. 3782–3790, 2018.
- [3] B. Sebastian and P. Ben-Tzvi, “Physics based path planning for autonomous tracked vehicle in challenging terrain,” *Journal of Intelligent & Robotic Systems*, vol. 95, no. 2, pp. 511–526, 2019.
- [4] H. Wu, Y. Chen, and H. Qin, “Mpc based trajectory tracking for an autonomous deep-sea tracked mining vehicle,” *ASP Transactions on Internet of Things*, vol. 1, no. 2, pp. 1–13, 2021.

- [5] J.-h. Han, C.-h. Park, Y. Y. Jang, J. D. Gu, and C. Y. Kim, "Performance evaluation of an autonomously driven agricultural vehicle in an orchard environment," *Sensors*, vol. 22, no. 1, p. 114, 2021.
- [6] I. Mahalingam and C. Padmanabhan, "A novel alternate multibody model for the longitudinal and ride dynamics of a tracked vehicle," *Vehicle System Dynamics*, vol. 59, no. 3, pp. 433–457, 2021.
- [7] H. Yang, X. Xu, and J. Hong, "Automatic parking path planning of tracked vehicle based on improved a* and dwa algorithms," *IEEE Transactions on Transportation Electrification*, 2022.
- [8] J. Wong and C. Chiang, "A general theory for skid steering of tracked vehicles on firm ground," *Proceedings of the Institution of Mechanical Engineers, Part D: Journal of Automobile Engineering*, vol. 215, no. 3, pp. 343–355, 2001.
- [9] S. Tang, S. Yuan, J. Hu, X. Li, J. Zhou, and J. Guo, "Modeling of steady-state performance of skid-steering for high-speed tracked vehicles," *Journal of terramechanics*, vol. 73, pp. 25–35, 2017.
- [10] Z. Liu, J. Guo, L. Ding, H. Gao, T. Guo, and Z. Deng, "Online estimation of terrain parameters and resistance force based on equivalent sinkage for planetary rovers in longitudinal skid," *Mechanical systems and signal processing*, vol. 119, pp. 39–54, 2019.
- [11] H. Taghavifar and S. Rakheja, "A novel terramechanics-based path-tracking control of terrain-based wheeled robot vehicle with matched-mismatched uncertainties," *IEEE Transactions on Vehicular Technology*, vol. 69, no. 1, pp. 67–77, 2019.
- [12] Z. Zhao, H. Liu, H. Chen, J. Hu, and H. Guo, "Kinematics-aware model predictive control for autonomous high-speed tracked vehicles under the off-road conditions," *Mechanical Systems and Signal Processing*, vol. 123, pp. 333–350, 2019.
- [13] J. Hu, Y. Hu, H. Chen, and K. Liu, "Research on trajectory tracking of unmanned tracked vehicles based on model predictive control (in chinese)," *Acta Armamentarii*, vol. 40, no. 3, p. 456, 2019.
- [14] A. Nikitin and L. Sergeev, "Teoriya tanka [tank theory]," Moscow, Izdaniye Akademii Bro-netankovykh voysk Publ, 1962.
- [15] A. D. Sabiha, M. A. Kamel, E. Said, and W. M. Hussein, "Ros-based trajectory tracking control for autonomous tracked vehicle using optimized backstepping and sliding mode control," *Robotics and Autonomous Systems*, vol. 152, p. 104058, 2022.
- [16] A. D. Sabiha, M. A. Kamel, E. Said and W. M. Hussein, "Dynamic modeling and optimized trajectory tracking control of an autonomous tracked vehicle via backstepping and sliding mode control," *Proceedings of the Institution of Mechanical Engineers, Part I: Journal of Systems and Control Engineering*, vol. 236, no. 3, pp. 620–633, 2022.
- [17] Z. Qin, L. Chen, J. Fan, B. Xu, M. Hu, and X. Chen, "An improved real-time slip model identification method for autonomous tracked vehicles using forward trajectory prediction compensation," *IEEE Transactions on Instrumentation and Measurement*, vol. 70, pp. 1–12, 2021.
- [18] M. Garber and J. Wong, "Prediction of ground pressure distribution under tracked vehicles—i. an analytical method for predicting ground pressure distribution," *Journal of Terramechanics*, vol. 18, no. 1, pp. 1–23, 1981.
- [19] D. Li, S. Wu, Y. Zhao, Z. Li, and J. Gong, "A hierarchical path tracking method for high-speed unmanned tracked vehicle," in *2021 IEEE International Intelligent Transportation Systems Conference (ITSC)*. IEEE, 2021, pp. 38–43.
- [20] R. Gonzalez, M. Fiacchini, T. Alamo, J. L. Guzman, and F. Rodriguez, "Adaptive control for a mobile robot under slip conditions using an lmi-based approach," *European Journal of Control*, vol. 16, no. 2, pp. 144–155, 2010.
- [21] Y. Dai, C. Xue, and Q. Su, "An Integrated Dynamic Model and Optimized Fuzzy Controller for Path Tracking of Deep-Sea Mining Vehicle," *Journal of Marine Science and Engineering*, vol. 9, no. 3, p. 249, 2021.
- [22] M. A. Subari, K. Hudha, Z. A. Kadir, S. M. Fairuz Syed Mohd Dardin, and N. H. Amer, "Development of Path Tracking Controller for An Autonomous Tracked Vehicle," in *2020 16th IEEE International Colloquium on Signal Processing & Its Applications (CSPA)*, 2020, pp. 126–130.
- [23] J. Jiao, L. Sun, W. Kong, Y. Zhang, Y. Qiao, and C. Yuan, "A sliding parameter estimation method based on UKF for agricultural tracked robot," in *The 2014 2nd International Conference on Systems and Informatics (ICSAI 2014)*, 2014, pp. 277–282.
- [24] H. Lu, G. Xiong, and K. Guo, "Motion Predicting of Autonomous Tracked Vehicles with Online Slip Model Identification," *Mathematical Problems in Engineering*, vol. 2016, pp. 1–13, 2016.
- [25] L. Rui and C. Li, "Slid parameter estimates for tracked vehicles with trajectory prediction compensation," *Journal of Tsinghua University(Science and Technology)*, vol. 62, no. 1, pp. 133–140, 2022.
- [26] H. Wang, Q. Wang, Q. Rui, J. Gai, G. Zhou, L. Wan, and F. Zhang, "Analyzing and testing verification the performance about high-speed tracked vehicles in steering process (in chinese)," *Journal of Mechanical Engineering*, vol. 50, no. 16, pp. 162–172, 2014.
- [27] M. Burke, "Path-following control of a velocity constrained tracked vehicle incorporating adaptive slip estimation," in *2012 IEEE International Conference on Robotics and Automation*, 2012, pp. 97–102.
- [28] J. Tao, H. Liu, Y. Li, H. Guan, J. Liu, and H. Chen, "Design of trajectory tracking controller of unmanned tracked vehicles based on torque control," in *2021 IEEE International Conference on Unmanned Systems (ICUS)*. IEEE, 2021, pp. 85–92.
- [29] J. Y. Wong, *Theory of ground vehicles*. John Wiley & Sons, 2022.
- [30] J. Y. Wong *et al.*, *Terramechanics and off-road vehicles*. Elsevier, 1989.
- [31] J. Gao and S. L. Zhang, "Path Tracking Control of Micro-Tracked Mobile Robot," *Applied Mechanics and Materials*, vol. 644–650, pp. 265–271, 2014.
- [32] X. Wang, J. Taghia, and J. Katupitiya, "Robust Model Predictive Control for Path Tracking of a Tracked Vehicle with a Steerable Trailer in the Presence of Slip," *IFAC-PapersOnLine*, vol. 49, no. 16, pp. 469–474, 2016.
- [33] A. D. Sabiha, M. A. Kamel, E. Said, and W. M. Hussein, "Trajectory Generation and Tracking Control of an Autonomous Vehicle Based on Artificial Potential Field and optimized Backstepping Controller," in *2020 12th International Conference on Electrical Engineering (ICEENG)*, 2020, pp. 423–428.
- [34] Q.-j. Han and S.-j. Liu, "Path tracking control of tracked vehicle," *International Journal of Computer Science Issues (IJCSI)*, vol. 10, no. 6, p. 103, 2013.
- [35] T. Hiramatsu, S. Morita, M. Pencelli, M. Niccolini, M. Ragaglia, and A. Argiolas, "Path-Tracking Controller for Tracked Mobile Robot on Rough Terrain," *International Journal of Electrical and Computer Engineering*, vol. 13, no. 2, pp. 59–64, 2019.
- [36] J. Lu, H. Liu, H. Guan, D. Li, H. Chen, and L. Liu, "Trajectory tracking control of unmanned tracked vehicles based on adaptive dual-parameter optimization (in chinese)," *Acta Armamentarii*, vol. 44, no. 4, p. 960, 2022.
- [37] S. Hong, J.-S. Choi, H.-W. Kim, M.-C. Won, S.-C. Shin, J.-S. Rhee, and H.-u. Park, "A path tracking control algorithm for underwater mining vehicles," *Journal of Mechanical Science and Technology*, vol. 23, no. 8, pp. 2030–2037, 2009.
- [38] T. Zou, J. Angeles, and F. Hassani, "Dynamic modeling and trajectory tracking control of unmanned tracked vehicles," *Robotics and Autonomous Systems*, vol. 110, pp. 102–111, 2018.
- [39] M. H. A. Sidi, K. Hudha, Z. A. Kadir, and N. H. Amer, "Modeling and path tracking control of a tracked mobile robot," in *2018 IEEE 14th International Colloquium on Signal Processing & Its Applications (CSPA)*, 2018, pp. 72–76.
- [40] N. Strawa, D. I. Ignatyev, A. C. Zolotas, and A. Tsourdos, "On-Line Learning and Updating Unmanned Tracked Vehicle Dynamics," *Electronics*, vol. 10, no. 2, p. 187, 2021.
- [41] M. Ahmad, V. Polotski, and R. Hurteau, "Path tracking control of tracked vehicles," in *Proceedings 2000 ICRA. Millennium Conference. IEEE International Conference on Robotics and Automation. Symposia Proceedings (Cat. No.00CH37065)*, vol. 3, 2000, pp. 2938–2943 vol.3.
- [42] T.-k. Yeu, S.-j. Park, S. Hong, H.-w. Kim, and J.-s. Choi, "Path Tracking using Vector Pursuit Algorithm for Tracked Vehicles Driving on the Soft Cohesive Soil," in *2006 SICE-ICASE International Joint Conference*, 2006, pp. 2781–2786.
- [43] D. Cui, G. Wang, H. Zhao, and S. Wang, "Research on a Path-Tracking Control System for Articulated Tracked Vehicles," *Strojniški vestnik – Journal of Mechanical Engineering*, vol. 66, no. 5, pp. 311–324, 2020.
- [44] S. Al-Milli, L. D. Seneviratne, and K. Althofer, "Track-terrain modelling and traversability prediction for tracked vehicles on soft terrain," *Journal of Terramechanics*, 2010.
- [45] A. T. Le, D. Rye, and H. Durrant-Whyte, "Estimation of track-soil interactions for autonomous tracked vehicles," in *Proceedings of International Conference on Robotics and Automation*, vol. 2, 1997, pp. 1388–1393 vol.2.
- [46] T. M. Dar and R. G. Longoria, "Slip estimation for small-scale robotic tracked vehicles," in *Proceedings of the 2010 American Control Conference*, 2010, pp. 6816–6821.
- [47] H. Huang, L. Zhai, and Z. Wang, "A Power Coupling System for Electric Tracked Vehicles during High-Speed Steering with Optimization-Based Torque Distribution Control," *Energies*, vol. 11, no. 6, p. 1538, 2018.
- [48] Z. Li, L. Chen, Q. Zheng, X. Dou, and L. Yang, "Control of a path following caterpillar robot based on a sliding mode variable structure algorithm," *Biosystems Engineering*, vol. 186, pp. 293–306, 2019.

- [49] X. Han, H. He, J. Wu, J. Peng, and Y. Li, "Energy management based on reinforcement learning with double deep Q-learning for a hybrid electric tracked vehicle," *Applied Energy*, vol. 254, p. 113708, 2019.
- [50] Y. Zou, T. Liu, D. Liu, and F. Sun, "Reinforcement learning-based real-time energy management for a hybrid tracked vehicle," *Applied Energy*, vol. 171, pp. 372–382, 2016.
- [51] Y. Zou, Z. Kong, T. Liu, and D. Liu, "A real-time markov chain driver model for tracked vehicles and its validation: Its adaptability via stochastic dynamic programming," *IEEE Transactions on Vehicular Technology*, vol. 66, no. 5, pp. 3571–3582, 2016.
- [52] H.-y. Wang, B. Chen, Q. Rui, J. Guo, and L.-c. Shi, "Analysis and experiment of steady-state steering of tracked vehicle under concentrated load(in chinese)," *Acta Armamentarii*, vol. 37, no. 12, p. 2196, 2016.
- [53] R. Zeng, Y. Kang, J. Yang, B. Qin, S. Chen, and D. Cao, "An Integrated Terrain Identification Framework for Mobile Robots: System Development, Analysis, and Verification," *IEEE/ASME Transactions on Mechatronics*, vol. 26, no. 3, pp. 1581–1590, 2021.
- [54] C. Dong, K. Cheng, W. Hu, and Y. Yao, "Dynamic modelling of the steering performance of an articulated tracked vehicle using shear stress analysis of the soil," *Proceedings of the Institution of Mechanical Engineers, Part D: Journal of Automobile Engineering*, vol. 231, no. 5, pp. 653–683, 2017.
- [55] M. N. Özdemir, V. Kılıç, and Y. S. Ünlüsoy, "A new contact & slip model for tracked vehicle transient dynamics on hard ground," *Journal of terramechanics*, vol. 73, pp. 3–23, 2017.
- [56] Y. Dai, X. Zhu, H. Zhou, Z. Mao, and W. Wu, "Trajectory Tracking Control for Seafloor Tracked Vehicle By Adaptive Neural-Fuzzy Inference System Algorithm," *International Journal of Computers Communications & Control*, vol. 13, no. 4, pp. 465–476, 2018.
- [57] Z. Janosi, "The analytical determination of drawbar pull as a function of slip for tracked vehicles in deformable soils," in *International Society for Terrain-Vehicle Systems, 1st Int. Conf.*, vol. 707, 1961.
- [58] J. Y. Wong, *Terramechanics and off-road vehicle engineering: terrain behaviour, off-road vehicle performance and design*. Butterworth-heinemann, 2009.
- [59] J. Wong and J. Preston-Thomas, "On the characterization of the shear stress-displacement relationship of terrain," *Journal of Terramechanics*, vol. 19, no. 4, pp. 225–234, 1983.
- [60] M. Bekker, "Off-road locomotion," *Ordnance*, vol. 53, no. 292, pp. 416–418, 1969.
- [61] D. Szpaczyńska, M. Łopatka, and P. Krogul, "The running gear construction impact on overcoming obstacles by light high-mobility tracked UGV," *Journal of Terramechanics*, vol. 112, pp. 1–17, 2024.
- [62] H. Dugoff, P. S. Fancher, and L. Segel, "An analysis of tire traction properties and their influence on vehicle dynamic performance," *SAE transactions*, pp. 1219–1243, 1970.
- [63] E. Bakker, L. Nyborg, and H. B. Pacejka, "Tyre modelling for use in vehicle dynamics studies," *SAE Transactions*, pp. 190–204, 1987.
- [64] K. Guo and D. Lu, "Unitire: unified tire model for vehicle dynamic simulation," *Vehicle System Dynamics*, vol. 45, no. S1, pp. 79–99, 2007.
- [65] S. Monsma *et al.*, *Feel the Tire-Tire Influence on Driver's Handling Assessment*. Aalto University, 2015.
- [66] Y. Zhang, S. Bei, B. Li, Y. Jin, and H. Yan, "A Review of the Research on the Mechanical Model of Vehicle Tires," in *Proceedings of the 2018 International Conference on Mechanical, Electrical, Electronic Engineering & Science (MEEES 2018)*. Atlantis Press, 2018.
- [67] M. Pearson, O. Blanco-Hague, and R. Pawłowski, "Tamatire: Introduction to the model," *Tire Science and Technology*, vol. 44, no. 2, pp. 102–119, 2016.
- [68] W. Hirschberg, G. Rill, and H. Weinfurter, "Tire model tmeasy," *Vehicle System Dynamics*, vol. 45, no. S1, pp. 101–119, 2007.
- [69] J. Dallas, M. P. Cole, P. Jayakumar, and T. Ersal, "Terrain adaptive trajectory planning and tracking on deformable terrains," *IEEE Transactions on Vehicular Technology*, vol. 70, no. 11, pp. 11255–11268, 2021.
- [70] C. Pavlov and A. M. Johnson, "A terramechanics model for high slip angle and skid with prediction of wheel-soil interaction geometry," *Journal of Terramechanics*, vol. 111, pp. 9–19, 2024.
- [71] Z. Jia, W. Smith, and H. Peng, "Terramechanics-based wheel–terrain interaction model and its applications to off-road wheeled mobile robots," *Robotica*, vol. 30, no. 3, pp. 491–503, 2012.
- [72] G. Ishigami, A. Miwa, K. Nagatani, and K. Yoshida, "Terramechanics-based model for steering maneuver of planetary exploration rovers on loose soil," *Journal of Field robotics*, vol. 24, no. 3, pp. 233–250, 2007.
- [73] O. A. Ani, B. Uzoejinwa, A. Ezeama, A. Onwualu, S. Ugwu, and C. Ohagwu, "Overview of soil-machine interaction studies in soil bins," *Soil and Tillage Research*, vol. 175, pp. 13–27, 2018.
- [74] J. Guo, T. Guo, M. Zhong, H. Gao, B. Huang, L. Ding, W. Li, and Z. Deng, "In-situ evaluation of terrain mechanical parameters and wheel-terrain interactions using wheel-terrain contact mechanics for wheeled planetary rovers," *Mechanism and Machine Theory*, vol. 145, p. 103696, 2020.
- [75] Z. Janosi and B. Hanamoto, "An analysis of the drawbar pull vs slip relationship for track laying vehicles," ARMY TANK-AUTOMOTIVE CENTER WARREN MI, Tech. Rep., 1961.
- [76] K. Guo, D. Lu, S.-k. Chen, W. C. Lin, and X.-p. Lu, "The UniTire model: A nonlinear and non-steady-state tyre model for vehicle dynamics simulation," *Vehicle System Dynamics*, vol. 43, pp. 341–358, 2005.
- [77] K. Guo, Y. Zhuang, D. Lu, S.-k. Chen, and W. Lin, "A study on speed-dependent tyre–road friction and its effect on the force and the moment," *Vehicle System Dynamics*, vol. 43, no. sup1, pp. 329–340, 2005.
- [78] A. Savkoor, "Some aspects of friction and wear of tyres arising from deformations, slip and stresses at the ground contact," *Wear*, vol. 9, no. 1, pp. 66–78, 1966.
- [79] M. G. Bekker, *Introduction to terrain-vehicle systems. part i: The terrain. part ii: The vehicle.* University of Michigan Press, 1969.
- [80] P. A. Dudziński and D. Stefanow, "Method for predicting dynamic shear strength in soils—part ii: Validation of the new criterion using an innovative test device," *Journal of Terramechanics*, vol. 86, pp. 39–46, 2019.
- [81] R. Zhang, W. Zhou, H. Liu, J. Gong, H. Chen, and A. Khajepour, "A terramechanics-based dynamic model for motion control of unmanned tracked vehicles," *IEEE Transactions on Intelligent Vehicles*, 2024.
- [82] M. G. Bekker, *Theory of land locomotion*. University of Michigan press, 1956.
- [83] O. Rauf, Y. Ning, C. Ming, and M. Haoxiang, "Evaluation of ground pressure, bearing capacity, and sinkage in rigid-flexible tracked vehicles on characterized terrain in laboratory conditions," *Sensors*, vol. 24, no. 6, p. 1779, 2024.